Applied Mathematical Modelling 144 (2025) 116061

Contents lists available at ScienceDirect

Applied Mathematical Modelling

journal homepage: www.elsevier.com/locate/apm

Moment-based Hermite model for asymptotically small non-Gaussianity

Vincent Denoël [a,b,*]

[a] University of Liège, Structural & Stochastic Dynamics, Belgium
[b] Stanford University, Department of Civil and Environmental Engineering, USA

ARTICLE INFO

Keywords:
Gram-Charlier series expansion
Edgeworth expansion
Monotonic region
Wind pressure
Reliability
Fatigue analysis

ABSTRACT

The third degree Moment-based Hermite model, which expresses a random variable as a cubic transformation of a standard normal variable, offers versatility in engineering applications. While its probability density function is not directly tractable, it is more complex to compute than the Gram-Charlier series, which, despite its simplicity, suffers from limitations such as positivity and unimodality issues, restricting its range of applicability. This paper presents two asymptotic analyses of the cubic Moment-based Hermite model for slight non-Gaussianity (i.e. small skewness and excess coefficients, "small" being understood in the sense of perturbation methods), showing that it asymptotically converges to the fourth cumulant Gram-Charlier model, while offering a slightly broader domain of applicability with minimal additional computational cost. Additionally, the paper derives, mathematically, a non empirical expression for the monotone limit of the original cubic translation model, and validates the theoretical findings through numerical simulations.

1. Introduction

Accurately modeling the probability density function (PDF) of a random variable using its moments is a cornerstone in both theoretical and applied statistics, with wide-reaching implications in fields such as structural engineering, finance, and meteorology.

Traditional approaches like the Gram-Charlier and Edgeworth series expansions have long been employed for this purpose [1]. These series expand the PDF around a Gaussian core, incorporating higher-order moments to account for skewness, kurtosis, and other non-Gaussian features [2]. However, despite their theoretical appeal, these expansions often suffer from significant practical limitations, particularly when applied to strongly non-Gaussian data or when truncated at higher orders [3]. These series expansions have found numerous applications in wind engineering [4], ocean engineering [5], meteorology [6], queueing theory [7], and financial sciences [8,9].

Alternative solutions exist to model non-Gaussian variables, such as the cubic translation model [10]. This model, originally developed to address the challenges of non-Gaussian modeling in fields such as wind engineering [11] and offshore mechanics [12], provides a more flexible framework that can accurately capture the tails and extreme values of a distribution [13,14]. Unlike the Gram-Charlier series, the cubic translation model does not rely on a series expansion around a Gaussian core but instead transforms a Gaussian variable into a non-Gaussian one using a cubic polynomial. It is therefore a four-parameter model. This transformation

* Correspondence to: University of Liège, Structural & Stochastic Dynamics, Belgium.
E-mail address: v.denoel@uliege.be.

https://doi.org/10.1016/j.apm.2025.116061
Received 3 October 2024; Received in revised form 1 March 2025; Accepted 3 March 2025

Available online 7 March 2025
0307-904X/© 2025 Elsevier Inc. All rights reserved, including those for text and data mining, AI training, and similar technologies.

allows for the modeling of asymmetry and kurtosis quite naturally, making it particularly useful in applications where extreme events play a critical role, such as in the assessment of structural reliability under random loads [15,16].

The Gram-Charlier and cubic translation models can be seen as two extremes, each with its own set of limitations. The Gram-Charlier model struggles with ensuring the positivity of the probability density function (PDF), while the cubic translation model is constrained by the monotonicity of the cubic transformation, which is generally less restrictive than the positivity issue in the Gram-Charlier model. However, we also argue that the cubic translation model is more time-consuming, particularly when fitting it to experimental data. This is because the moments are related to the model parameters through nonlinear algebraic equations that must be solved numerically [17]. While this might not be a significant concern when only a single fitting is needed, this additional computational burden becomes problematic in several scenarios, as detailed next.

First, simulating samples from non-Gaussian processes can be time-consuming. Early simulation methods (e.g. [18]) are suitable to generate small samples sizes. The use in the context of large non-Gaussian fields [19] may take up to several hours of computation. This challenge is further amplified when long samples are required to analyze fatigue damage and extreme values [20]. Second, modern applications, with a typically much higher space resolution than used some decades ago, demand far more fittings than in the past. Repeating fittings across entire fields, especially in marginal or extended bivariate cases of the bicubic model [21,22], also results in significant data processing delays. Lastly, this issue is exacerbated when learning methods are integrated into the process [23], as high-quality training sets typically require thousands of independent simulations.

A significant portion of the research focuses on refining and applying Gram-Charlier (also called Hermite polynomial) models. Recent advancements, such as the use of proper parametrized probability distribution model [24], quartic Hermite models [25] and probability-weighted moment-based Hermite models [26], have demonstrated improvements in the modeling performance of methods bases on the Hermite polynomial. Additionally, a simplified analytical formula for the coefficient of the third-order Hermite moment model has been developed [27].

Variables with large skewness and excess can be effectively modeled using mixtures of less non-Gaussian variables [22]. This is easy to understand, as, for example, significantly skewed variables can be generated by mixing two (symmetric) Gaussian variables [28]. In extreme cases with strongly skewed distributions, an enhanced expression of the fourth-order moment method can also be applied [29].

The range of possible applications is therefore quite broad and multiple techniques have been developed recently to improve the Gram-Charlier model in the significantly non-Gaussian domain. In this work, we explore another area where improvements can be made: specifically, at the opposite end of the spectrum, where the modeled variable is only slightly non-Gaussian, i.e. with small skewness and excess. This area, apparently less appealing, has been relatively less explored as the current models provide interesting modeling options. In such cases, a simple moment-based approach like the Gram-Charlier models proves to be more computationally efficient than the cubic translation model, which requires the solution of nonlinear algebraic equations. However its domain of positivity might still remain restrictive, even in the small non-Gaussian domain, and this is where this contribution stands.

Building on these observations, this paper specializes the cubic translation model in the domain of small non-Gaussianity, by developing its asymptotic version with a tractable PDF (without any nonlinear algebraic equation to be solved), albeit with a reduced range of applicability in terms of the high skewness and kurtosis offered by the original model. We pursue two main objectives: first, to conduct a comparative analysis between the Gram-Charlier series and the cubic translation model, identifying the conditions under which each method yields the most accurate and physically meaningful results; second, to develop a new asymptotic model for the cubic translation model in the degenerate case, where non-Gaussianity is weak but still significant. Specifically, we investigate the potential for deriving simple analytical expressions for the PDF that depend on only a few moments, preserving the benefits of moment-based methods while addressing their limitations. Although Hermite polynomial models are available for both softening and hardening processes [30], this paper focuses exclusively on softening models, for which the cubic translation model was first derived.

After outlining the key features of the Gram-Charlier series and the cubic translation process in Sections 2 and 3 respectively, the asymptotic version of the cubic translation model is derived in Section 4. Comparative illustrations are given in Section 5. The potential improvements offered by the proposed method are also demonstrated through an example of wind load on the roof of a low-rise building.

2. The Gram-Schmidt expansion model

It is not uncommon in probability theory to encounter situations where the moments of a random variable can be determined, but the PDF itself remains elusive. The Gram-Charlier series expansion provides an approximate representation of the PDF based on the first few moments. In experimental practice, a large amount of data is required to infer moments beyond the fourth order with sufficient confidence. In this work, it is therefore supposed that the skewness coefficient γ_3 and the excess coefficient $\gamma_e = \gamma_4 - 3$ are known. Furthermore, in probabilistic modeling, a four-parameter model is typically versatile enough to accommodate various types of data.

More specifically, the Gram-Charlier series expansion expresses the PDF of a non-Gaussian variable as

$$p_{\mathrm{GC}}(x) = \frac{1}{\sigma}\left[1 + \frac{\gamma_3}{3!}\mathcal{H}_3\left(\frac{x-\mu}{\sigma}\right) + \frac{\gamma_e}{4!}\mathcal{H}_4\left(\frac{x-\mu}{\sigma}\right)\right]\phi\left(\frac{x-\mu}{\sigma}\right) \tag{2.1}$$

where μ and σ are the average and standard deviation, γ_3 and γ_e are the skewness and excess coefficients, $\phi(\cdot)$ is the normalized Gaussian PDF, and $\mathcal{H}_3(\xi) = \xi^3 - 3\xi$ and $\mathcal{H}_4(\xi) = \xi^4 - 6\xi^2 + 3$ are Hermite polynomials. This model offers a simple analytical expression for the PDF. However, it has notable limitations: for certain values of skewness and excess, the resulting PDF may become negative over

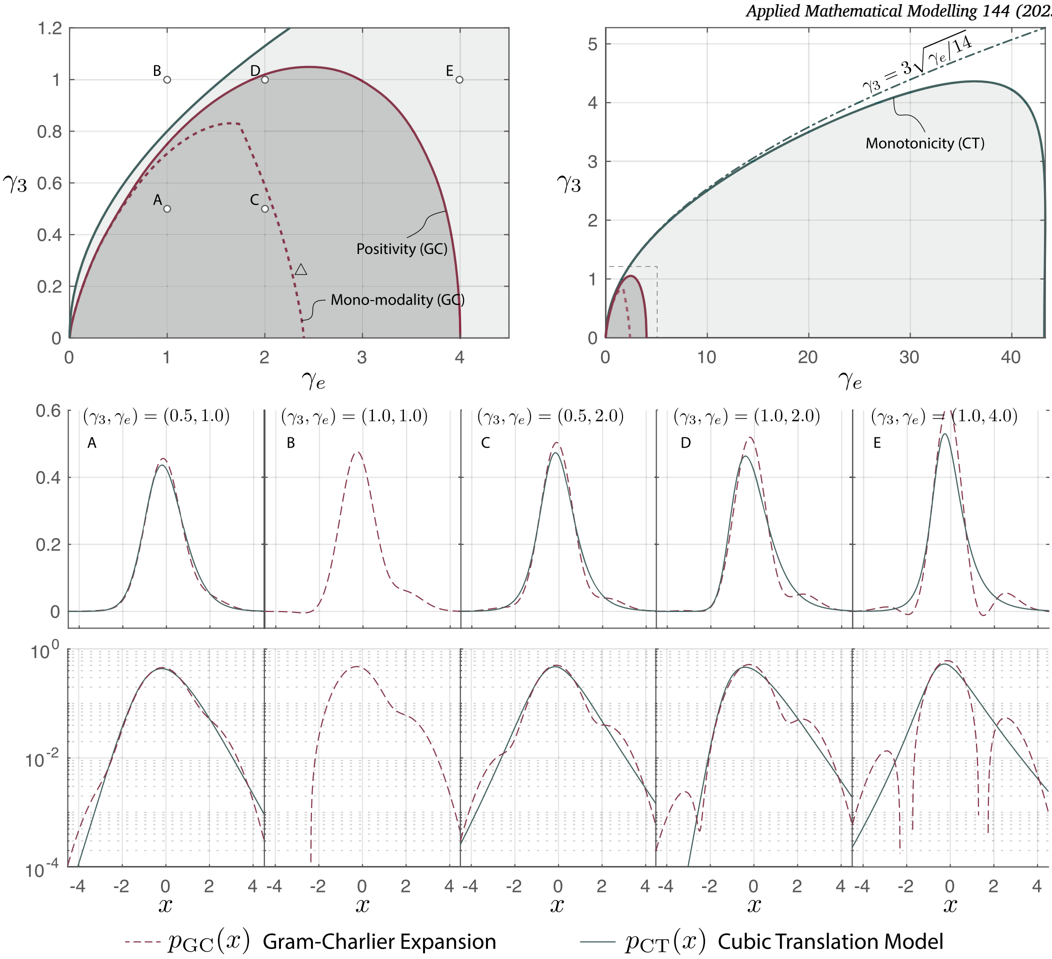

Fig. 2.1. (Top) Limits of the 4th-cumulant Gram-Charlier series expansion model (GC) and of the cubic translation model (CT); (Bottom) examples of PDFs for various values of (γ_3, γ_e) in linear and log scales. Selected values: $\mu = 0$, $\sigma = 1$, and (γ_3, γ_e) changing from case A to case E.

some range or exhibit multiple modes, reducing its physical validity [3,31]. Furthermore, the series' convergence is not guaranteed, and in some cases, it may fail to provide a meaningful approximation, particularly for distributions with heavy tails or sharp peaks [32]. Despite these challenges, the Gram-Charlier series remains a widely used tool, primarily due to its straightforward connection to the moments and its ease of computation, especially when truncated at low order, on when the effective domain of interest is on a finite interval [33,34].

A challenge, therefore, lies in identifying the regions of the parameter space where the Gram-Charlier series remains both positive definite and unimodal [31]. Although this task could appear difficult with the computational means available in 1950, some corrections of early results have been provided later [3,35], and reported in Fig. 2.1 where the thick solid and dashed lines represent the respective boundaries of the domain where the PDF is positive and unimodal. This figure also shows some illustrations of $p_{GC}(x)$ for various sets of pairs (γ_3, γ_e) and $\mu = 0$, and $\sigma = 1$.

3. The cubic translation model

The cubic translation model [12] expresses the process to be modeled as a cubic transformation of a normalized Gaussian process $u(t)$,

$$x(u) = \mu + \alpha u + \frac{\alpha}{b}\left(\frac{u^3}{3} + au^2 - u - a\right) \tag{3.1}$$

parameterized by the four parameters (μ, α, a, b). The centered moments of the resulting random variable are

$$\mathbb{E}\left[(x-\mu)^2\right] = \frac{\alpha^2}{b^2}\left(2a^2 + b^2 + \frac{2}{3}\right) = \sigma^2$$

$$\mathbb{E}\left[(x-\mu)^3\right] = \frac{\alpha^3}{b^3}2a\left(4a^2 + 3b^2 + 6b + 6\right)$$

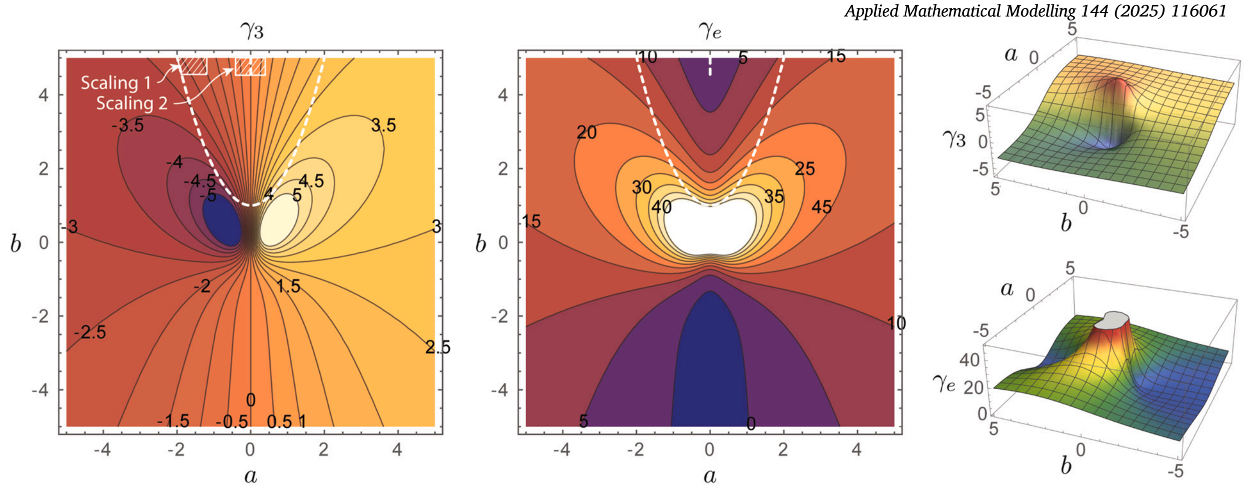

Fig. 3.1. Illustration of the relations $\gamma_3(a,b)$ and $\gamma_e(a,b)$, as given by Equations (3.3) and (3.4), with $\alpha \geq 0$.

$$\mathbb{E}\left[(x-\mu)^4\right] = \frac{\alpha^4}{b^4}\left(60a^4 + 4a^2\left(15b^2+48b+62\right) + 3b^4 + 8b^3 + 28b^2 + 48b + \frac{124}{3}\right) \tag{3.2}$$

with $\mathbb{E}[x] = \mu$, the expectation of variable x. Following the definition of the skewness and kurtosis coefficients, $\gamma_n = \mathbb{E}\left[(x-\mu)^n\right]/\sigma^n$ for $n \in \{3,4\}$, it is found that they are expressed as a function of a and b only, α being simplified out:

$$\gamma_3 = \frac{2a\left(4a^2+3b^2+6b+6\right)}{\left(2a^2+b^2+\frac{2}{3}\right)^{3/2}}\operatorname{sign}\alpha \tag{3.3}$$

$$\gamma_4 = \gamma_e + 3 = \frac{60a^4 + 4a^2\left(15b^2+48b+62\right) + 3b^4 + 8b^3 + 28b^2 + 48b + \frac{124}{3}}{\left(2a^2+b^2+\frac{2}{3}\right)^2} \tag{3.4}$$

Therefore, the skewness γ_3 and excess $\gamma_e = \gamma_4 - 3$ can be used to determine the values of parameters a and b, while the average provides μ, and α is determined from the second moment. The set of equations mapping $\left(\gamma_3, \gamma_e\right)$ onto (a,b) is illustrated in Fig. 3.1. It is significantly nonlinear and can only be solved numerically. Several formulas provide closed-form but approximate solutions to that set of equations [13,36]. This figure also shows that the Gaussian case, obtained in the limiting case for vanishing γ_3 and γ_e, corresponds to $b \to +\infty$, which is also confirmed by Equation (3.1).

Using the principles of transformation of random variables [37], the probability density function (PDF) of process $x(t)$ is then given by

$$p_{\mathrm{CT}}(x) = u'(x)\phi\left[u(x)\right] = \frac{b}{\alpha}\frac{\phi\left[u(x)\right]}{u^2(x) + 2au(x) + b - 1} \tag{3.5}$$

where the reverse mapping

$$u(x) = \sqrt[3]{\zeta + \sqrt{c+\zeta^2}} + \sqrt[3]{\zeta - \sqrt{c+\zeta^2}} - a \tag{3.6}$$

is expressed as a function of $c = \left(b-1-a^2\right)^3$ and

$$\zeta(x) = \frac{3b}{2}\left(a + \frac{x-\mu}{\alpha}\right) - a^3. \tag{3.7}$$

This result requires the cubic transformation (3.1) to be monotonic, a condition that is satisfied provided $b-1-a^2 \geq 0$ [12]. Fig. 2.1b illustrates the versatility of this model, as shown by the domain of validity in the $\left(\gamma_3, \gamma_e\right)$ plane, significantly larger than for the fourth cumulant Gram-Charlier model. A clear advantage of this approach is that $p_{\mathrm{CT}}(x)$ does not suffer from positivity issues, as a result of the process of its definition. As soon as the monotonicity condition is met (all but case 'B'), the cubic translation model apparently provides smoother PDFs, as illustrated in the lower panels of Fig. 2.1.

4. The slightly non-Gaussian cubic translation model

The Gram-Charlier series and the cubic translation model are two powerful tools in probabilistic modeling. While the Gram-Charlier series offers a simple analytical expression for the PDF, its applicability is limited by a narrow domain of validity. In contrast, the cubic translation model features a broader domain of validity, though its PDF is more complex, making certain operations—such as the addition of two such random variables—challenging to manage. Motivated by this and the observation that many practical problems can be effectively modeled with variables exhibiting slight deviations from Gaussianity, we develop in this Section the asymptotic behavior of the cubic translation model in these scenarios. Two particularly significant distinguished limits are detailed in this section, along with their associated scaling.

4.1. Generalities common to the two scaling options

In the asymptotic limit where the skewness and excess coefficients are small, the process only slightly deviates from Gaussianity ($\alpha \to \sigma$, $b \to \infty$), and the cubic transformation (3.1) and its inverse (3.6) tend to the linear transformations $x = \mu + \sigma u$ and $u = (x-\mu)/\sigma$, respectively. Therefore, instead of the complicated relation (3.6), we will use the asymptotic series

$$u(x) = u_0(x) + \varepsilon u_1(x) + \varepsilon^2 u_2(x) + \mathcal{O}\left(\varepsilon^3\right) \cdots \tag{4.1}$$

where $0 < \varepsilon \ll 1$ is a small number explicitly introduced in the mathematical derivation to sort out the terms with various orders of magnitude, and where $u_0(x)$, $u_1(x)$, $\cdots$ are obtained by solving (3.1) for u with standard perturbation techniques, see e.g. [38]. As seen in the following, this results in u_i's being expressed as polynomials of x, instead of cubic roots. In particular, the unperturbed case ($\gamma_3 = 0$, $\gamma_e = 0$) corresponds to $u_0 = (x-\mu)/\sigma$.

To obtain the asymptotic expression for $p_{\text{CT}}(x)$, the derivative $u'(x)$ is computed from (4.1), and $\phi[u(x)]$ is expanded as

$$\phi(u) \sim \phi\left(u_0\right) + \left(u-u_0\right)\partial_u\phi\left(u_0\right) + \frac{1}{2}\left(u-u_0\right)^2\partial_u^2\phi\left(u_0\right) + \mathcal{O}\left(\varepsilon^3\right) \tag{4.2}$$

$$= \phi\left(u_0\right) + \varepsilon\left(u_1 + \varepsilon u_2\right)\partial_u\phi\left(u_0\right) + \frac{1}{2}\varepsilon^2 u_1^2\partial_u^2\phi\left(u_0\right) + \mathcal{O}\left(\varepsilon^3\right). \tag{4.3}$$

Noticing that $\partial_u\phi\left(u_0\right) = -u_0\phi\left(u_0\right)$ and $\partial_u^2\phi\left(u_0\right) = -\phi\left(u_0\right) + u_0^2\phi\left(u_0\right)$ as ϕ is the normalized Gaussian PDF, we also have

$$\phi(u) = \left[1 - \varepsilon u_0 u_1 - \frac{1}{2}\varepsilon^2\left(u_1^2 - u_0^2u_1^2 + 2u_0u_2\right)\right]\phi\left(u_0\right) + \mathcal{O}\left(\varepsilon^3\right). \tag{4.4}$$

Combining (4.1) and (4.4), the asymptotic expansion of $p_{\text{CT}}(x)$ is

$$p_{\text{CT}}(x) = \left(u_0' + \varepsilon\left(u_1' - u_0u_0'u_1\right) + \varepsilon^2\left(u_2' + \frac{1}{2}u_0^2u_0'u_1^2 - \frac{1}{2}u_0'u_1^2 - u_0u_0'u_2 - u_0u_1u_1'\right)\right)\phi\left(u_0\right) + \mathcal{O}\left(\varepsilon^3\right). \tag{4.5}$$

Interestingly when u_i's are indeed polynomials, this formulation is similar (but not identical to) to the general Gram-Charlier formulation: a polynomial multiplying the standard Gaussian distribution.

Two scaling options are considered in the following. They are supported by the fact that, in the asymptotic Gaussian case, $b \to \infty$, while there is no strict condition on a, except the monotonicity condition, $a \le \sqrt{b-1}$. Therefore, two zones of the acceptable (a,b)-region are analyzed, see hatched areas in Fig. 3.1. The first is near the monotone limit, where $b \sim a^2 \sim \varepsilon^{-1}$. The second is near the central part of this region where only b is large and a remain of order 1.

4.2. Scaling 1

A first distinguished limit is achieved by considering the scaling

$$a = \frac{\bar{a}}{\varepsilon} \quad ; \quad b = \frac{\bar{b}}{\varepsilon^2} \tag{4.6}$$

where $\bar{a} \sim 1$ and $\bar{b} \sim 1$ are both of order 1 at most. Substitution of these expressions in the moments (3.2) provides the following asymptotic expansions for the skewness and excess coefficients

$$\gamma_3 = 6\frac{\bar{a}}{\bar{b}}\varepsilon + \mathcal{O}\left(\varepsilon^3\right) \quad ; \quad \gamma_e = \frac{8\left(6\bar{a}^2 + \bar{b}\right)}{\bar{b}^2}\varepsilon^2 + \mathcal{O}\left(\varepsilon^4\right). \tag{4.7}$$

Under the scaling (4.6), the skewness is therefore of order ε and the excess, much smaller, of order ε^2. This formulation is ideal to study the area near to the boundary of the monotonic region, for small non-Gaussianity. Indeed, as seen in Fig. 2.1, the excess is much smaller than the skewness on the boundary of the monotone region. After truncation of the previous equations to leading order, and elimination of ε in favor of a and b, solving the two previous equations for a and b yields

$$a = \frac{4\gamma_3}{3\gamma_e - 4\gamma_3^2} \quad ; \quad b = \frac{24}{3\gamma_e - 4\gamma_3^2}, \tag{4.8}$$

so that substitution into the equation for the boundary of the monotonic region, $b - 1 - a^2 = 0$, and solving for γ_e gives

$$\gamma_e = \frac{4}{3}\left(\gamma_3^2 - \sqrt{9-\gamma_3^2} + 3\right) = \frac{14}{9}\gamma_3^2 + \mathcal{O}\left[\gamma_3^3\right]. \tag{4.9}$$

Now the approached expression for the PDF is developed following the general method presented in Section 4.1. With the considered scaling, the cubic transformation (3.1) becomes

$$x = \mu + \alpha u_0 + \alpha\varepsilon \left(\frac{\bar{a}\left(u_0^2 - 1\right)}{\bar{b}} + u_1 \right) + \alpha\varepsilon^2 \left(\frac{6\bar{a}u_1 + u_0^2 - 3}{3\bar{b}} u_0 + u_2 \right) + \mathcal{O}\left(\varepsilon^3\right). \tag{4.10}$$

Balancing and canceling the similar powers in ε, as in standard perturbation methods, the reverse mapping $u(x)$ is

$$u(x) = u_0 + \varepsilon u_1 + \varepsilon^2 u_2 + \cdots = \xi + \varepsilon \frac{\bar{a}}{\bar{b}} \left(1 - \xi^2\right) + \varepsilon^2 \left(\frac{\xi^3}{3} \frac{6\bar{a}^2 - \bar{b}}{\bar{b}^2} - \xi \frac{2\bar{a}^2 - \bar{b}}{\bar{b}^2} \right) + \mathcal{O}\left(\varepsilon^3\right) \tag{4.11}$$

where $\xi = (x - \mu)/\alpha$. Finally, substitution of these expressions for u_0, u_1 and u_2 into (4.5), elimination of ε, and replacement of (a, b) by $\left(\gamma_3, \gamma_e\right)$ through (4.8), the general solution (4.5) specializes into

$$p_{\mathrm{CT}}^{(1)}(x) = \left[p_{\mathrm{CT}}^{(\mathrm{Ref})}(\xi(x)) + \frac{\gamma_3^2}{72\alpha} \left(\xi^6 - 15\xi^4 + 47\xi^2 - 17\right) \right] \phi(\xi(x)) \tag{4.12}$$

where ξ needs to be understood as $\xi(x)$, and

$$p_{\mathrm{CT}}^{(\mathrm{Ref})}(\xi) = 1 + \frac{\gamma_3}{3!}\xi\left(\xi^2 - 3\right) + \frac{\gamma_e}{4!}\left(\xi^4 - 6\xi^2 + 3\right). \tag{4.13}$$

In these expressions, α is similar to the standard deviation σ of the process to be modeled, but is estimated from (3.2), with the values of a and b obtained from (4.8).

4.3. Scaling 2

A second interesting scaling consists in assuming

$$a \sim 1 \qquad ; \qquad b = \frac{\tilde{b}}{\varepsilon} \tag{4.14}$$

in which case the skewness and excess coefficients now read

$$\gamma_3 = \frac{6a}{\tilde{b}}\varepsilon + \frac{12a}{\tilde{b}^2}\varepsilon^2 + \mathcal{O}\left(\varepsilon^3\right) \qquad ; \qquad \gamma_e = \frac{8}{\tilde{b}}\varepsilon + \frac{24\left(1 + 2a^2\right)}{\tilde{b}^2}\varepsilon^2 + \mathcal{O}\left(\varepsilon^3\right). \tag{4.15}$$

In this formulation, both γ_3 and γ_e have the same order of magnitude. Unfortunately, truncating these series after the second term and solving for a and $\tilde{b}$ does not lead to a simple expression. The only option to express them in a consistent manner is to truncate after leading term, which leads

$$a = \frac{4\gamma_3}{3\gamma_e} \qquad ; \qquad b = \frac{8}{\gamma_e}. \tag{4.16}$$

Substitution into $b - 1 - a^2 = 0$ yields

$$\frac{8}{\gamma_e} - 1 - \frac{16\gamma_3^2}{9\gamma_e^2} = 0 \tag{4.17}$$

whose solution is $\gamma_e = \frac{4}{3}\left(3 - \sqrt{9 - \gamma_3^2}\right) \sim \frac{2}{9}\gamma_3^2$. Although it appears quite similar to (4.9), the final expression of the limit is fundamentally different. This is explained by the fact that, in this second scaling, γ_3 and γ_e do not have the appropriate order of magnitude (both of order ε) to capture the trend $\gamma_3 \sim \pm\sqrt{\gamma_e}$ of the boundary of the monotonic region.

However, this scaling is meant to be appropriate inside the domain of validity of the cubic translation model, where both the skewness and the excess coefficients are small and of the same order of magnitude. So instead of focusing on the limit of the monotonic region, we rather seek to develop a second approximation $p_{\mathrm{CT}}^{(2)}(x)$. To do this the reverse of the mapping is first obtained as in the previous case, by introducing the ansatz $u(x) = u_0 + \varepsilon u_1 + \varepsilon^2 u_2 + \cdots$ into the definition of the mapping, and considering the re-scaling of b, which yields

$$x = \mu + \alpha u_0 + \alpha\varepsilon \left(\frac{a\left(u_0^2 - 1\right) + \frac{u_0^3}{3} - u_0}{\tilde{b}} + u_1 \right) + \alpha\varepsilon^2 \left(\frac{2au_0 + u_0^2 - 1}{\tilde{b}} u_1 + u_2 \right) + \mathcal{O}\left(\varepsilon^3\right) = 0. \tag{4.18}$$

Again, cancellation of each and every power of ε yields, successively,

$$u_0 = \frac{x - \mu}{\alpha} = \xi; \qquad u_1 = \frac{1}{\tilde{b}}\left(\xi - \frac{\xi^3}{3} + a\left(1 - \xi^2\right)\right); \qquad u_2 = \frac{1}{3\tilde{b}^2}\left(\left(\xi^2 + 2a\xi - 1\right)\left(3a\left(\xi^2 - 1\right) + \xi\left(\xi^2 - 3\right)\right)\right). \tag{4.19}$$

These quantities can be substituted into (4.5) to obtain, after some simplifications, the second sought expansion of the PDF of the slightly non Gaussian cubic translation process

$$p_{\mathrm{CT}}^{(2)}(x) = \left[p_{\mathrm{CT}}^{(\mathrm{Ref})}(\xi(x)) + \frac{\gamma_3^2}{72\alpha}\left(\xi^6 - 11\xi^4 + 23\xi^2 - 5\right) + \frac{\gamma_3\gamma_e}{144\alpha}\xi\left(\xi^6 - 15\xi^4 + 51\xi^2 - 33\right) + \frac{\gamma_e}{1152\alpha}\left(\xi^8 - 19\xi^6 + 93\xi^4 - 117\xi^2 + 18\right)\right]\phi(\xi(x)). \quad (4.20)$$

Since the first two corrections to leading have been considered in the expansions, this approached PDF is quadratic in γ_3 and γ_e, a distinctive feature of this model.

5. Discussion

The primary objective of this study was to explore the feasibility of deriving simple analytical expressions for the probability density function (PDF) of a non-Gaussian random variable, characterized by its first few moments. This exploration began with the cubic translation model, recognized for its broad domain of validity in the (γ_3, γ_e)-plane.

The first asymptotic analysis of the cubic translation model yielded results where the skewness γ_3 and excess γ_e were of orders ε and ε^2, respectively, and resulted in the simple expression $\gamma_3 = 3\sqrt{\gamma_e/14}$ for the boundary of the monotonic region, for small non-Gaussianity. This expression is accurate in a significantly wide domain of the (γ_3, γ_4)-plane, since the subsequent terms in (4.7) are two orders of magnitude smaller. This expression is confirmed by Fig. 2.1, where the dashed dotted line on the right indicates a strong agreement between this analytical expression and the numerical results represented by the solid green line. To the author's knowledge, it is the first time that an expression for the boundary of the monotonic region is obtained from analytical derivations. Interestingly, when rewritten as $\gamma_e = \frac{14}{9}\gamma_3^2$, it is very close to the empirical fitting $\gamma_e = \left(1.25\gamma_3\right)^2$ provided by Winterstein and McKenzie [14], as $1.25^2 \simeq 1.5625$ while $14/9 \simeq 1.5556$ in the current equation.

The derived PDF for the slightly non-Gaussian variable $p_{\mathrm{CT}}^{(1)}(x)$, expressed as a sixth-degree polynomial multiplied by the standard Gaussian PDF $\phi(\cdot)$, shares some similarities with the Gram-Charlier series.

In contrast, the second asymptotic analysis did not exhibit the same convergence properties, as the first correction to the leading term was only one order of magnitude smaller, see (4.15). This discrepancy limits the accuracy of this approach in capturing the boundary of the monotonic region, despite the apparent similarity between the formulations (4.9) and (4.17). Nevertheless, the slower convergence of the sequence in ε does not preclude the derivation of a more precise PDF for the slightly non-Gaussian cubic translation process. Indeed, the resulting PDF, $p_{\mathrm{CT}}^{(2)}(x)$, represented as an eighth-degree polynomial multiplied by the standard Gaussian PDF $\phi(\cdot)$, effectively extends the applicability of the Gram-Charlier approach within the (γ_3, γ_4)-plane. This is demonstrated in the following section by means of numerical simulations. For symmetry reasons, the upper half of the $\left(\gamma_3, \gamma_e\right)$ plane only is studied, for $\gamma_3 > 0$; the lower half can be obtained by replacing γ_3 by $-\gamma_3$.

Both asymptotic expressions converge to $p_{\mathrm{CT}}(x) \sim p_{\mathrm{CT}}^{(\mathrm{Ref})}[\xi(x)]\,\phi(\xi(x))$ as $(\gamma_3, \gamma_e) \to 0^+$, which coincides with the Gram-Charlier PDF $p_{\mathrm{GC}}(x)$. In this limit, coefficients of powers of x greater than 4 vanish, and the parameter α approaches σ, rendering the cubic translation model asymptotic to the fourth-degree truncated Gram-Charlier series.

The Gram-Charlier series employs an n-degree polynomial strictly expressed as a function of the first n statistical moments. However, our approach results in an eighth-degree polynomial dependent on moments up to the fourth, with the additional four degrees of freedom derived from lower moments. As seen in $p_{\mathrm{CT}}^{(1)}(x)$ and $p_{\mathrm{CT}}^{(2)}(x)$, these coefficients are not proportional to the cumulants as in the Gram-Charlier model but can also be expressed as higher powers of lower cumulants. Indeed, by incorporating the first two corrections to the leading term, the resulting PDF is quadratic in γ_3 and γ_e. This approach offers two key advantages: (1) it circumvents the need to measure higher-order moments to obtain higher degree polynomials, which are often impractical, and (2) it reduces the dimensionality of the parameter space, making the derived expression more tractable and applicable.

6. Illustrations

6.1. Positivity and unimodality

For expressions like the Gram-Charlier series, the limits of validity (positivity of the PDF, and to a lesser extent, the unimodality) can be conveniently obtained by means of numerical simulations. Indeed for given μ and σ, and for a chosen pair of parameters (γ_3, γ_4), the PDF $p_{\mathrm{GC}}(x)$ can be computed with (2.1). To limit chances of missing a zero-crossing located far away from the bulk of the density, we computed $p_{\mathrm{GC}}(x)$ for 5,000 uniformly spaced values of x in the interval $[\mu - 35\sigma; \mu + 35\sigma]$. Positivity was checked by comparing the values to zero. Unimodality was checked by computing the 1-step finite difference of this PDF and detecting the number of sign changes. Unimodality was concluded if one and only one sign change had been observed. By repeating this operation for 600×600 values of γ_3 and γ_e uniformly spaced between 0 and 1.2, and 0 and 4.5, the plots of Figs. 2.1 and 6.1 could be established. Indeed with such a fine mesh on γ_3 and γ_e, the limits of the positivity region (solid lines) and unimodality region (dashed lines) can just be obtained with standard contouring features of scientific softwares. The same operation was repeated for $p_{\mathrm{CT}}^{(1)}(x)$ and $p_{\mathrm{CT}}^{(2)}(x)$, with (4.13) and (4.20).

While the bottom of Fig. 6.1 shows some examples of the PDF of the fourth degree Gram-Charlier model, and the two proposed asymptotic expansions, the top part of the Figure summarizes the major findings of this study, both in linear and log scales. The grayed area recalls the positivity boundary of the fourth degree Gram-Charlier model, for comparison.

The first asymptotic model suffers positivity issues as soon as $\gamma_3 > 0.7$, whereas the Gram-Charlier model can manage skewness coefficients slightly larger than 1, provided the excess lies between 2 and 3. This might be seen as a weakness of the proposed model

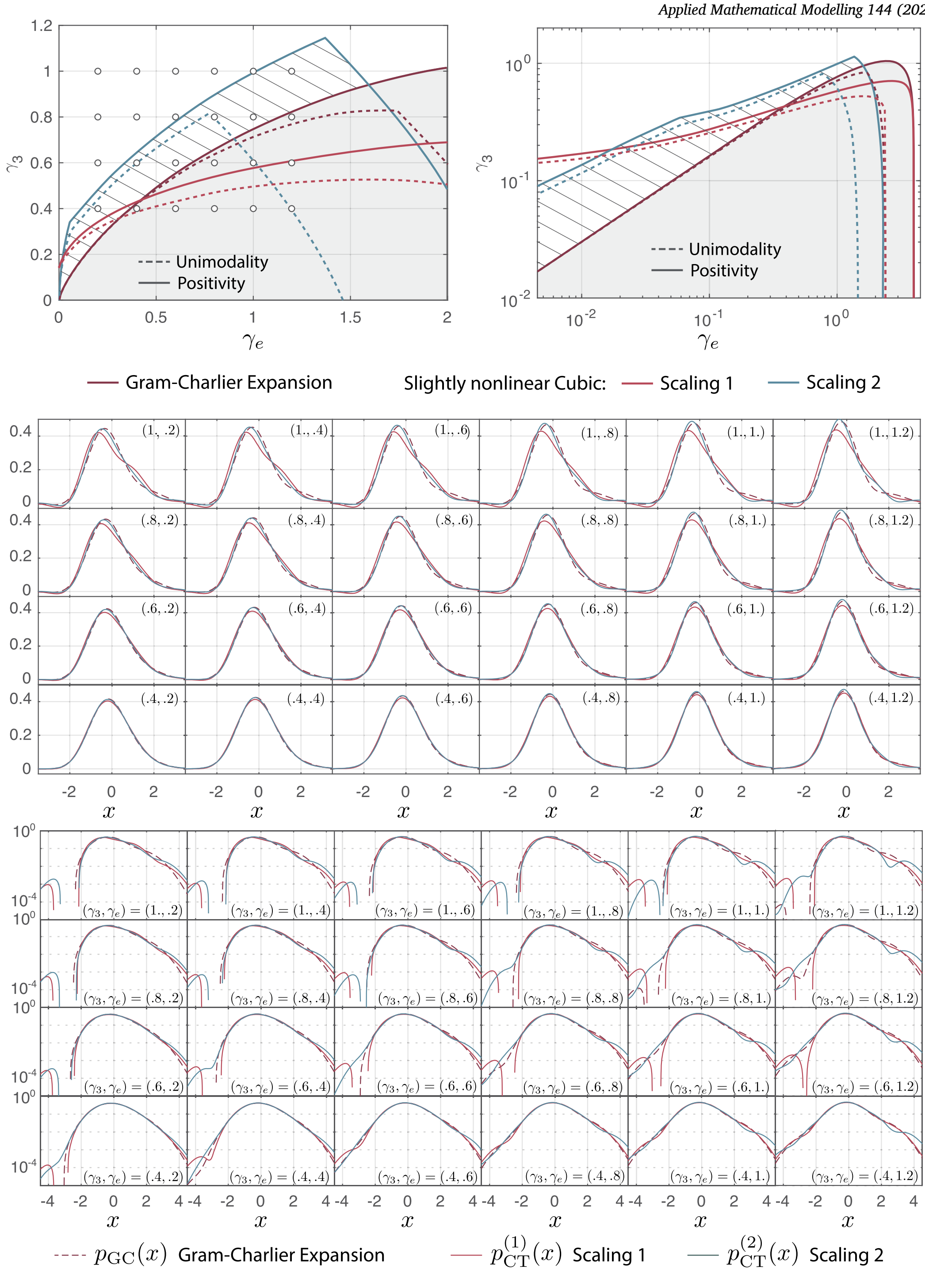

Fig. 6.1. Limits of the 4th-degree Gram-Charlier series expansion model and of the two proposed asymptotic models. Represented in terms of positivity (solid lines) and unimodality (dashed lines). Bottom: some selected illustrations of the corresponding PDFs. White dots in the upper right plot locate these selected combinations of (γ_3, γ_e). Shown for $\mu = 0$, $\sigma = 1$.

expressed as the product of a 6-th degree polynomial and the standard Gaussian PDF. However, it is noticed that the first asymptotic model is valid for zero excess, up to a skewness coefficient as large as $\gamma_3 = 0.2$, while the Gram-Charlier model would not allow $\gamma_3 \neq 0$ if $\gamma_e = 0$. The dots represented on the uniform mesh on the top left plot locate the various combinations (γ_3, γ_4) illustrated at the bottom. The logarithmic scale on the y-axis makes it easier to identify positivity and unimodality issues. For instance, for $(\gamma_3, \gamma_4) = (.4, .4)$, all three compared models result in positive PDF, $p_{\mathrm{CT}}^{(1)}(x)$ is not unimodal. In general, $p_{\mathrm{CT}}^{(1)}(x)$ is more bumpy than

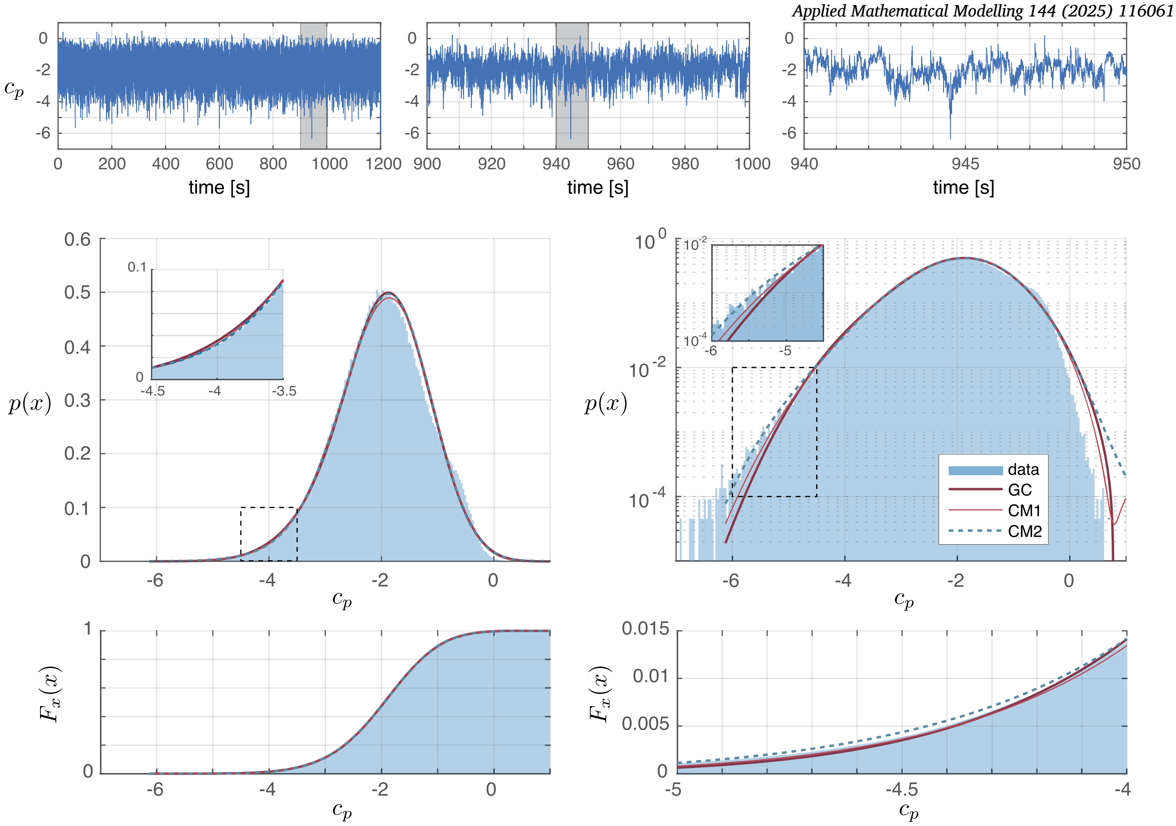

Fig. 6.2. Illustration of the fitting of the different types of models to wind pressure data: (top) time series, (middle) PDFs, (bottom) cumulative density functions (CDFs).

$p_{GC}(x)$ and does not bring much added value, except perhaps in the small area where γ_e is very small and γ_3 can reach values up to $\gamma_3 = 0.2$.

Our second asymptotic model performs actually much better. The hatched area indicates the zone where the Gram-Charlier model is extended. For $\gamma_e < 1.5$, it roughly shows a shift of the boundary of the positivity region, of about 0.25 units on the γ_3-axis. This difference could seem marginal but is appreciable since (i) again, zero excess does not require zero skewness, (ii) we can now offer skewness coefficients as large as 1, when γ_e lies between 1 and 1.6, a great complementary to the Gram-Charlier model. Furthermore, in the numerous cases where $p_{CT}^{(2)}(x)$ is positive while $p_{GC}(x)$ is not, see e.g. $(\gamma_3, \gamma_4) \in \{(.6, .6), (.8, .8), (.8, 1.)\}$, the shape of $p_{CT}^{(2)}(x)$ is rather smooth and could therefore be appealing for modeling purposes. Last but not least, for $\gamma_3 = 0.4$, the second asymptotic model $p_{CT}^{(2)}(x)$ and the Gram-Charlier model $p_{GC}(x)$ are virtually superimposed.

6.2. Illustration with wind pressure time series

Fig. 6.2 shows the time series of wind pressure measured on the roof of a low-rise building (from [39]). This time series is selected to illustrate that pressure coefficients on buildings can exhibit slight non-Gaussian behavior. In other areas of the roof and/or building, the skewness may be more pronounced, and clearer signs of bimodality may appear in the data. These features would require a different statistical treatment than the one proposed in this paper. The mixed nature of the data is also partly evident here, with a noticeable bump in the experimental probability density function —the histogram of the pressure coefficient— near $c_p = -1$. This feature cannot be captured by the model discussed in this paper, which explains why pressure coefficients near zero are not appropriately captured by the models compared here. On the other tail, however, the proposed model performs well. It accurately models the bulk of the distribution, which is the primary goal of a moment-based approach, and the versatility provided by using moments up to the fourth order ensures that this good agreement extends fairly far into the tail. This is further confirmed by the close-up view of both the tails of the PDFs and the cumulative density functions (CDFs). The log-scale representation of the PDFs (right panel in the middle) shows that the second asymptotic distribution (CM2) provides an excellent match with the experimental PDF down to probability densities as small as 10^{-4}, more than three orders of magnitude smaller than the density in the bulk of the distribution. Nevertheless the quality of the match is poorer near $c_p = 4.5$ and shown on the CDFs.

The skewness and excess of this time series are $\gamma_3 = -0.3194$ and $\gamma_e = 0.1823$, which form a combination where the second asymptotic distribution (CM2) meets the positivity criterion, while the Gram-Charlier (GC) and first asymptotic distribution (CM1)

Table 1
Near tail α-fractiles computed with the experimental CDF, and the CDF of the Gram-Charlier (GC) model, and the two proposed asymptotic models (CM1, CM2).

α	Exp.	GC	CM1	CM2
0.1000	-3.0765	-3.0713 (-0.17%)	-3.0727 (-0.13%)	-3.0680 (-0.28%)
0.0500	-3.4230	-3.4343 (0.33)	-3.4215 (-0.04)	-3.4214 (-0.05)
0.0200	-3.8390	-3.8558 (0.44)	-3.8338 (-0.14)	-3.8469 (0.21)
0.0100	-4.1353	-4.1342 (-0.03)	-4.1195 (-0.38)	-4.1521 (0.41)
0.0050	-4.4034	-4.3830 (-0.46)	-4.3852 (-0.41)	-4.4442 (0.92)
0.0010	-5.0383	-4.8749 (-3.24)	-4.9263 (-2.22)	-5.0399 (0.03)
0.0005	-5.2930	-5.0591 (-4.42)	-5.1291 (-3.10)	-5.2558 (-0.70)
0.0002	-5.6471	-5.2830 (-6.45)	-5.3722 (-4.87)	-5.5063 (-2.49)

do not. In this case, both distributions become negative for some $c_p > 0$. In this example this does not impact the modeling of large extreme negative values, which are in the other tail.

One way to quantify the appropriateness of the model in reproducing the statistics of large negative wind pressures is by comparing the fractiles associated with non-exceedance probabilities for certain thresholds with small probability α. Some of these fractiles are provided in Table 1, along with the errors computed by referencing the experimental data. Once again, the second asymptotic distribution is shown to perform overall pretty well, except near $c_p = 4.5$ (around 1%-discrepancy) and in the tail, where $\alpha \sim 10^{-4}$ and where experimental data may suffer from sampling issues.

7. Conclusions

This study investigated the cubic translation model as a robust alternative to the Gram-Charlier series for modeling non-Gaussian random variables, particularly in engineering applications with small skewness and kurtosis.

The first asymptotic expansion of the cubic translation model focused on solutions near the boundary of the monotonic region, providing a simple yet effective analytical expression for the PDF of slightly non-Gaussian variables. This model is especially useful in cases of near-zero excess, extending the range of skewness coefficients where the PDF remains valid. However, for larger skewness values, the first asymptotic model begins to lose its advantage, struggling to maintain unimodality and positivity, which the Gram-Charlier series handles more effectively. Nonetheless, a key strength of this approach is its ability to accurately estimate the limit of the monotone region in the original cubic translation model, which was expressed as $\gamma_3 = \pm 3\sqrt{\gamma_e/14}$, an expression that is very close to commonly used formula derived from fitting.

The second asymptotic expansion offered significant improvements over both the Gram-Charlier series and the first expansion. It extended the positivity region and produced smoother PDF shapes, making it a more practical and versatile tool for modeling slight non-Gaussianity. Notably, the second model was able to handle skewness coefficients as large as 1, particularly in regions where the Gram-Charlier series fails. However, for $\gamma_3 = 1$, the proposed model breaks down, and the Gram-Charlier expansion becomes more suitable for $\gamma_3 \in [2; 3]$. Therefore, the cubic translation model provides a complementary approach, expanding the range of skewness-excess combinations that can be effectively modeled.

The derived PDFs are expressed as the product of a polynomial and the standard Gaussian PDF. The degree of the polynomial (six or eight) is higher than that of the truncated fourth-cumulant Gram-Charlier series (four), and its coefficients are no longer proportional to cumulants. This opens the door for further exploration of other variants with similar structures. Although the domain of applicability in the (γ_3, γ_e)-plane is significantly reduced compared to original cubic translation model, the slightly non Gaussian cubic translation model enters in the family of distributions having a “polynomial times Gaussian PDF” format. Since it is tractable and allows for simpler computations, the model derived in this paper can benefit from fast estimation, since the PDF is expressed by means of statistics moments. Any subsequent quantity such as a likelihood or posterior distribution in a Bayesian inference context is therefore much easier to obtain than for the original cubic translation model.

Declaration of competing interest

The authors declare that they have no known competing financial interests or personal relationships that could have appeared to influence the work reported in this paper.

Acknowledgements

This work was partly carried out during a UPS Visiting Professor appointment at Stanford University, for which the author is deeply grateful.

Data availability

Data will be made available on request.

References

[1] H. Anders, The early history of the cumulants and the Gram-Charlier series, Int. Stat. Rev. 68 (2) (2000) 137–153.
[2] S. Blinnikov, R. Moessner, Expansions for nearly Gaussian distributions, Astron. Astrophys. Suppl. Ser. 130 (1) (1998) 193–205.
[3] N.R. Draper, D.E. Tierney, Regions of positive and unimodal series expansion of the Edgeworth and Gram-Charlier approximations, Biometrika 59 (2) (1972) 463–465.
[4] I. Gullo, G. Muscolino, M. Vasta, Non-Gaussian probability density function of SDOF linear structures under wind actions, J. Wind Eng. Ind. Aerodyn. 74–76 (1998) 1123–1134.
[5] M. Choi, B. Sweetman, The Hermite moment model for highly skewed response with application to tension leg platforms, J. Offshore Mech. Arct. Eng. 132 (2) (2010) 021602.
[6] L. Mahmoudi, W. Wang, N. Ikegaya, Comparing annual extreme winds in Iran predicted by numerical weather forecasting and Gram-Charlier statistical model with meteorological observation data, Build. Environ. 261 (2024).
[7] J. Pender, Gram Charlier expansion for time varying multiserver queues with abandonment, SIAM J. Appl. Math. 74 (4) (2014) 1238–1265.
[8] T.-M. Ñíguez, J. Perote, Moments expansion densities for quantifying financial risk, N. Am. J. Econ. Finance 42 (2017) 53–69.
[9] M.G. Zoia, P. Biffi, F. Nicolussi, Value at risk and expected shortfall based on Gram-Charlier-like expansions, J. Bank. Finance 93 (2018) 92–104.
[10] S.R. Winterstein, Moment-based Hermite models of random vibration, Afdelingen for bærende konstruktioner, Danmarks tekniske højskole, 1987.
[11] F. Wu, M. Liu, Q. Yang, L. Peng, Estimation of extremes of non-Gaussian wind pressure on building roof: Sampling error in moment-based translation process model with no monotonic limit, Adv. Struct. Eng. 23 (4) (2020) 810–826.
[12] S.R. Winterstein, Nonlinear vibration models for extremes and fatigue, J. Eng. Mech. 114 (10) (1988) 1772–1790.
[13] S.R. Winterstein, T. Kashef, Moment-based load and response models with wind engineering applications, J. Sol. Energy Eng. 122 (3) (2000) 122–128.
[14] S.R. Winterstein, C.A. MacKenzie, Extremes of nonlinear vibration: Comparing models based on moments, L-moments, and maximum entropy, J. Offshore Mech. Arct. Eng. 135 (2) (2013) 021602.
[15] M. Gioffrè, V. Gusella, M. Grigoriu, Non-Gaussian wind pressure on prismatic buildings. II: Numerical simulation, J. Struct. Eng. 127 (9) (2001) 990–995.
[16] L. Yang, K.R. Gurley, D.O. Prevatt, Probabilistic modeling of wind pressure on low-rise buildings, J. Wind Eng. Ind. Aerodyn. 114 (2013) 18–26.
[17] K.R. Gurley, M.A. Tognarelli, A. Kareem, Analysis and simulation tools for wind engineering, Probab. Eng. Mech. 12 (1) (1997) 9–31.
[18] M. Gioffrè, V. Gusella, M. Grigoriu, Simulation of non-Gaussian field applied to wind pressure fluctuations, Probab. Eng. Mech. 15 (4) (2000) 339–345.
[19] Y. Li, J. Xu, An efficient methodology for simulating multivariate non-Gaussian stochastic processes, Mech. Syst. Signal Process. 209 (2024).
[20] X.-Y. Zhang, Y.-G. Zhao, Z.-H. Lu, Unified Hermite polynomial model and its application in estimating non-Gaussian processes, J. Eng. Mech. 145 (3) (2019).
[21] V. Denoël, T. Bastin, G. Pomaranzi, A. Zasso, A bivariate statistical model of large pressure peaks measured in wind tunnel tests, in: Conference of the Italian Association for Wind Engineering, Springer, 2022, pp. 288–297.
[22] F. Rigo, T. Andrianne, V. Denoël, On the use of the cubic translation to model bimodal wind pressures, Math. Modell. Civ. Eng. 15 (2) (2019).
[23] J. Wang, X. Zheng, Q. He, Artificial intelligence applied to extreme value prediction of non-Gaussian processes with bandwidth effect and non-monotonicity, in: 2021 IEEE International Conference on Artificial Intelligence and Computer Applications (ICAICA), IEEE, 2021, pp. 721–727.
[24] C. Dang, J. Xu, Novel algorithm for reconstruction of a distribution by fitting its first-four statistical moments, Appl. Math. Model. 71 (2019) 505–524.
[25] Y.-G. Zhao, T. Wang, X. Ji, G. Huang, Quartic Hermite polynomial model-based translation method for extreme wind load estimation, J. Wind Eng. Ind. Aerodyn. 245 (2024).
[26] Y. Li, J. Xu, Novel Hermite polynomial model based on probability-weighted moments for simulating non-Gaussian stochastic processes, J. Eng. Mech. 150 (4) (2024).
[27] W. Chen, Y. Tian, A simplified analytical formula for the coefficient of 3rd-order Hermite moment model and its application, J. Wind Eng. Ind. Aerodyn. 254 (2024).
[28] R. Calif, PDF models and synthetic model for the wind speed fluctuations based on the resolution of Langevin equation, Appl. Energy 99 (2012) 173–182.
[29] L.-W. Zhang, An improved fourth-order moment reliability method for strongly skewed distributions, Struct. Multidiscip. Optim. 62 (3) (2020) 1213–1225.
[30] F. Wu, G. Huang, M. Liu, Simulation and peak value estimation of non-Gaussian wind pressures based on Johnson transformation model, J. Eng. Mech. 146 (1) (2020).
[31] D.E. Barton, K.E. Dennis, The conditions under which Gram-Charlier and Edgeworth curves are positive definite and unimodal, Biometrika 39 (3/4) (1952) 425–427.
[32] W. Wei, S. Koki, I. Naoki, Modelling probability density functions based on the Gram-Charlier series with higher-order statistics: Theoretical derivation and application, J. Wind Eng. Ind. Aerodyn. 231 (2022) 105227.
[33] W. Lin, J.E. Zhang, The valid regions of Gram–Charlier densities with high-order cumulants, J. Comput. Appl. Math. 407 (2022) 113945.
[34] W. Lin, K. Shen, J.E. Zhang, Further exploration into the valid regions of Gram–Charlier densities, J. Comput. Appl. Math. 429 (2023).
[35] O.K. Kwon, Analytic expressions for the positive definite and unimodal regions of Gram-Charlier series, Commun. Stat., Theory Methods 51 (15) (2022) 5064–5084.
[36] X. Peng, L. Yang, E. Gavanski, K. Gurley, D.O. Prevatt, A comparison of methods to estimate peak wind loads on buildings, J. Wind Eng. Ind. Aerodyn. 126 (2014) 11–23.
[37] A. Papoulis, S.U. Pillai, Probability, Random Variables, and Stochastic Processes, fourth edition, McGraw Hill, Boston, 2002.
[38] C.M. Bender, S.A. Orszag, Advanced Mathematical Methods for Scientists and Engineers, McGraw-Hill, 1978.
[39] N. Blaise, T. Andrianne, V. Denoël, Assessment of extreme value overestimations with equivalent static wind loads, J. Wind Eng. Ind. Aerodyn. 168 (2017) 123–133.